Springer

Journal of
Mechanical
Science and
Technology

Journal of Mechanical Science and Technology 22 (2008) 699~707

www.springerlink.com/content/1738-494x

Ultrasonic focused waveform generation using time reversal acoustic focusing system

Bok Kyoung Choi[1,*], Bong-Chae Kim[1], Alexander Sutin[2] and Armen Sarvazyan[2]

[1]*Korea Ocean Research and Development Institute 1270, Sa-2-dong, Sangrok-gu, Ansan-si, Gyeonggi-do, 426-744, Korea*

[2]*ARTANN Laboratories, 1459 Lower Ferry Road, Trenton, New Jersey 08618, USA*

(Manuscript Received September 12, 2006; Revised December 13, 2007; Accepted December 13, 2007)

Abstract

The concept of Time Reversal Acoustics (TRA) provides an elegant possibility of both temporal and spatial concentrating of acoustic energy in highly inhomogeneous media. We explored the possibility of generating acoustical signals with arbitrary waveforms using the TRA Focusing System (TRA FS). A method has been developed to predict TRA-focused ultrasound waveforms and spatial distribution by using the measurements of transfer function of transfer function relating the signal at the TRA transmitter to that at the focusing point.

The developed approach for TRA-focused signal waveform prediction from the results of direct signal measurements was tested on ten-channel TRA FS based on aluminum resonator with glued piezotransducers. The TRA FS operated in the frequency band of 100-1000 kHz.

The formation of ultrasonic signals with various envelopes was demonstrated experimentally. The calculated and experimentally measured waveforms and spatial distributions were practically identical. We formed triangular, rectangular, and amplitude modulated tone burst signals with different modulation frequencies in the focal region. The level of side lobes in the generated signals was much lower than that for standard TRA focusing.

Keywords: Ultrasound; Time reversal acoustics; Focusing; Impulse response; Deconvolution

1. Introduction

The ultrasound focusing systems based on time reversal acoustic (TRA) principles are capable of delivering ultrasound energy to a chosen region in a highly inhomogeneous medium (including soft tissues and bones) with focusing efficacy hardly achievable using a conventional phased array transmitter. Furthermore, numerous reflections from boundaries, which distort focusing in conventional ultrasound focusing systems and are viewed as a significant technical hurdle, lead to improvement of the focusing ability of the TRA system. TRA principles are described in review papers of Fink, the inventor of TRA, and his associates [1-3]. The TRA Focusing Systems (TRA FS) are able to focus and stir ultrasound beams in a 3D volume using just a few piezoceramic transducers glued to the facets of a solid (aluminum) block. The TRA FS can be applied to biomedical imaging [4-6], nondestructive testing [7-10], and land mine detection [11-13]. The prediction of the TRA-focused signals and the formation of the focused signals with desired form and frequency content is important for these and other TRA FS applications. Some experimental results demonstrating the ability of the TRA FS to produce various waveforms are presented in [14] and the current work considers how the TRA-focused field can be predicted and how TRA FS can form desired ultrasonic waves. The developed methods are based on the measurements of transfer function relating the signal at the TRA transmitter to that at the focusing point.

*Corresponding author. Tel.: +82 31 400 6118, Fax.: +82 31 408 5829
E-mail address: bkchoi@kordi.re.kr
DOI 10.1007/s12206-007-1203-6

2. Basic concepts of time-reversed focusing

The transmitter of the time reversal system is composed of an array of piezotransducers coupled with a metal resonator which radiates ultrasonic waves into the resonator (Fig. 1). The resonator is coupled with the tested media, and ultrasonic waves can penetrate from the resonator to this media. A hydrophone measures acoustic pressure in the tested area and the recorded signal is used for the TRA procedure consisting of the following sequence of steps:

Step 1. A wide-bandwidth initial signal *e(t)* with normalized amplitude (*max(e(t))=1)* is sequentially sent to each transducer.

Step 2. The long reverberation signal is recorded by the hydrophone placed in a chosen point of focus-ing in the tested media. There are two sources of reverberation: the first source is the resonator of the TRA transmitter where ultrasound signal experiences numerous reflections, and additional reverberation takes place at the boundaries of the tested media.

The *j*th transducer generates a signal at the hydrophone $s_j(t)$ that is connected with radiated signal by an expression:

$$s_j(t) = e(t) \otimes h_j(t) , \tag{1}$$

where $h_j(t)$ is the transfer function between the electrical signal applied to the *j*th transducer and the output of the hydrophone, a nd ⊗ indicates linear convolution.

The Fourier transformation of Eq. (1) has the form

$$S_j(\omega) = E(\omega)\ H_j(\omega) , \tag{2}$$

where $E(\omega)$, $H_j(\omega)$ and $S_j(\omega)$ are spectra of $e(t)$, $h_j(t)$ and $s_j(t)$ correspondingly.

Step 3. The recorded signal is time reversed and normalized, channel by channel for all *N* transducers (*j=1:N*) . The normalization maintains the same peak amplitude for all radiated signals. This normalization should be appropriately taken for the limitation of voltage that can be applied to a power amplifier for signal radiation. The time reversal signals prepared for reradiation have the form:

$$r_j(t) = \frac{s_j(t_{delay} - t)}{\max[s_j(t)]} , \tag{3}$$

where t_{delay} is an arbitrary delay chosen to ensure causality.

Step 4. All prepared TRA signals $r_j(t)$ are broadcasted over all transducers simultaneously. The measured TRA-focused signal associated with the *j*th transducer can be expressed as

$$p_j(t) = r_j(t) \otimes h_j(t) , \tag{4}$$

$$r_j(t) = \frac{s_j(t_{delay} - t)}{\max[s_j(t)]} .$$

In the frequency domain this formula has the form:

$$P_j(\omega) = \frac{E^*(\omega)\ H^*{}_j(\omega)\exp(i\omega t_{delay})H_j(\omega)}{\max[s_j(t)]} \tag{5}$$

We use here the following relationship:

$$FFT[s_j(t_{delay} - t)] = S_j^*(\omega)\exp(i\omega t_{delay})$$

Since the TRA signals are applied simultaneously to all transducers, the total response is given by the superposition of the individual responses.

$$p_{tot}(t) = \sum_{j=1}^{N} r_j(t) \otimes h_j(t) \tag{6}$$

3. Prediction of the TRA-focused field based on transfer function measurements

The linear relationship between radiated and recorded signals allows prediction of the acoustic field produced by the TRA-focused signal from the measurements of direct signals. The direct signals can be measured by any simple acoustic recording system and there is no need for application of a complex TRA system.

The direct signals at a chosen point can be defined as $s_j(t)$ (*j=1:N)*.

The spectrum of impulse responses can be expressed from Eq. (2)

$$H_j(\omega) = \frac{S_j(\omega)}{E\ (\omega)} \tag{7}$$

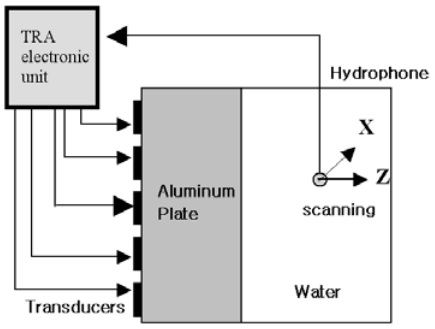

Fig. 1. Schematic diagram of the time reversal experiment.

and substitution to (5) gives the TRA-focused field for single transducer radiation:

$$P_j(\omega) = \frac{S^*{}_j(\omega)S_j(\omega)\exp(i\omega t_{delay})}{E(\omega)\max[s_j(t)]} \quad (8)$$

The waveform of the TRA-focused signal can be calculated by summation of spectra produced by all transducers and calculation of inverse FFT:

$$p_{tot}(t) = F^{-1}\left(\sum_{j=1}^{N}\frac{S^*{}_j(\omega)S_j(\omega)\exp(i\omega t_{delay})}{E(\omega)\max[s_j(t)]}\right) \quad (9)$$

There F^{1} indicates inverse Fourier transformation.

For a short initial signal that can be approximated as delta function $e(t) = A\delta(t)$ the radiated signal has the flat spectrum $E(\omega) = E_0 = A/2\pi$. Here E_0 is spectral density of the radiated signal.

In this case the spectrum of the focused field has the form:

$$P_j(\omega) = \frac{S^*{}_j(\omega)S_j(\omega)\exp(i\omega t_{delay})}{E_0\max[s_j(t)]} \quad (10)$$

Inverse Fourier transformation gives the temporal form of the received signal:

$$p_j(t) = \frac{[s_j(t-t_{delay}) * s_j(t-t_{delay})]}{E_0\max[s_j(t)]} \quad (11)$$

The summation of these signals for all transducers gives the total TRA-focused signal:

$$p_{tot}(t) = \sum_{j=1}^{N}\frac{[s_j(t-t_{delay}) * s_j(t-t_{delay})]}{E_0\max[s_j(t)]} \quad (12)$$

where q is a regularization parameter and it is chosen to be a constant value.

The autocorrelation of the direct signal gives the temporal form of the TRA signal as it is shown in [15]. It means that in many cases the waveform of the TRA-focused signal can be estimated by calculation of the autocorrelation of the recorded direct signal.

The direct application of Eq. (9) for calculation of the TRA field is problematic because the spectrum of the initial signal $E(\omega)$ is concentrated in a limited frequency band $(\omega_1 < \omega < \omega_2)$ and $E(\omega)$ is close to zero out of this frequency band. Because $E(\omega)$ is in the denominator of Eq. (9), small values of $E(\omega)$ can give large errors in calculation of the acoustic field. This deconvolution problem is generally ill posed and a solution does not uniquely exist. The regularization method based on Wiener filter [16, 17] can be used for approximate calculation of a TRA-focused field. In this case the whole spectrum without restriction ($0 < \omega < \pi$F, where F is the signal record sampling frequency) can be used.

The estimation of the TRA-focused field can be expressed in the form:

$$p_{tot}(t) = F^{-1}\left(\sum_{j=1}^{N}\frac{S^*{}_j(\omega)S_j(\omega)E^*(\omega)\exp(i\omega t_{delay})}{[E^*(\omega)E(\omega)+q]\max[s_j(t)]}\right) \quad (13)$$

where q is a regularization parameter and it is given a constant value.

The spatial distribution of the TRA-focused field can be also determined through measurements of the direct signal at various points. Let us consider a case where the direct signal is focused to the point *A* and the measured recorded direct signal produced by transducer *j* is s^A_j. We want to know the waveform of this signal at a different point *B*. This waveform can be found if we know the direct signal at this point s^B_j. Knowledge of direct signals allows us to determine the transfer function from the point of radiation to the measured point. The spectrum of the field in point *B,* when TRA focusing is conducted to the point *A,* is given by the expression,

$$P_{tot}(\omega) = \sum_{j=1}^{N}\frac{[S^A_j(\omega)]^* S^B_j(\omega)\exp(i\omega t_{delay})}{E(\omega)\max[s_j(t)]} \quad (14)$$

and the inverse FFT of this expression allows us to calculate spatial distribution of the TRA-focused field.

4. Comparison of predicted TRA-focused field with experiment

A schematic diagram of the time-reversed focusing experiment is shown in Fig. 1. The TRA resonator is made of aluminum and has dimensions of 90 x 60 x 120 mm^3. Five piezoceramic disk transducers (diameter 50 mm, thickness 3 mm) are glued to the external wall of the resonator. The opposite wall of the resonator is glued to the wall of a small water tank having size $90 \times 120 \times 120$ mm^3. The ultrasound signal in the tank is recorded by a needle-type hydrophone. A positioning system controlled by PC is used for hydrophone scanning.

For signal generating and reversing, we use the multi channel TRA system developed by Artann Laboratories. The system covers a wide frequency band (50 kHz–5 MHz) and provides the complete TRA procedure described above.

Snap shots of the signals in the process of the TRA

focusing are presented in Fig. 2. In this test we used the initial signal with an envelope in the form of half period of sinusoid with duration 45 μs with carrier frequency of 500 kHz wave, as it is shown in Fig. 2(a).

The typical spatial distribution of the TRA-focused signal amplitude for frequency 500 kHz is presented in Fig. 3. Fig. 4 shows spatial distribution along axis X (see Fig. 1) of the focused signal amplitude for different frequencies (250 kHz, 500 kHz and 1 MHz). It is seen that the focal spot decreases if frequency increases. The focal spot width is about half of the wavelength.

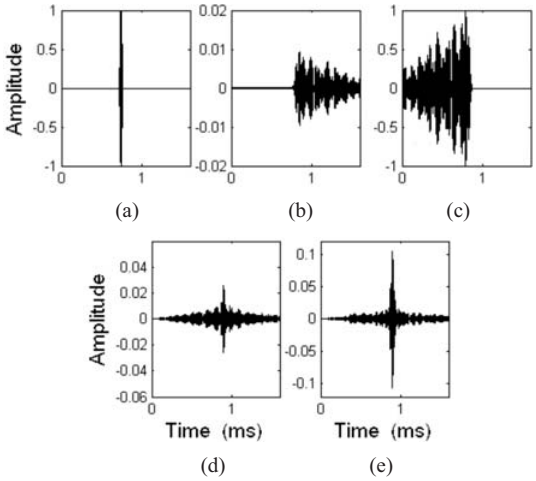

Fig. 2. The snap shots of the signals in the process of TRA focusing of tone burst pulse with carrier frequency 500 kHz: a) step 1 - initial radiated signal e(t), b) step 2 – recorded long reverberating signal, c) step 3 – time reversal normalized signal prepared for reradiation, d) TRA-focused signal radiated by single transducer, e) TRA-focused signal radiated by all five transducers.

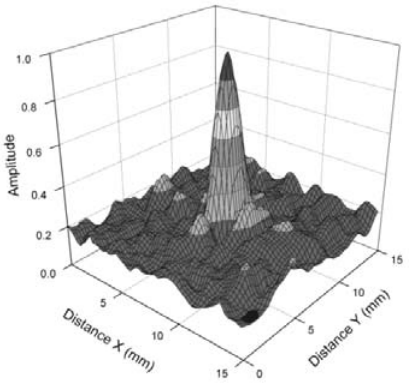

Fig. 3. Spatial distribution of the TRA-focused signal amplitude for tone burst with carrier frequency of 500 kHz.

As we described above, the prediction of the TRA focusing can be conducted by using the records of a direct signal. The simplest approximate prediction of the TRA focusing can be done by calculation of auto-correlation of the direct recorded signal as it is given by Eq. (11) The calculated approximate TRA-focused signals are shown in Fig. 5(b) and are seen to be close to the signal measured in the experiment Fig. 2(a) or Fig. 5(a).

The more accurate prediction of the form and amplitude of the TRA-focused signal can be done by using Eq. (13). The question is how to choose the regularization parameter q for best description of the TRA-focused signal.

For choosing of this parameter we can calculate the transfer function of the system and use this transfer function for estimation of the direct signal. In the case of the correct choice of the regularization parameter the estimated direct signal should be close to the measured one.

The transfer function spectrum , $H_{est}(\omega)$, can be estimated as

$$H_{est}(\omega) = S(\omega)\frac{E(\omega)^*}{E(\omega)^* E(\omega) + q}, \tag{15}$$

Then the estimated receiving signal, $S_{est}(\omega)$ is given by

$$s_{est}(t) = F^{-1}[E(\omega)H_{est}(\omega)]. \tag{16}$$

Fig. 5 shows the result of calculation of estimated transfer function and estimated direct signals for different values of parameter q .

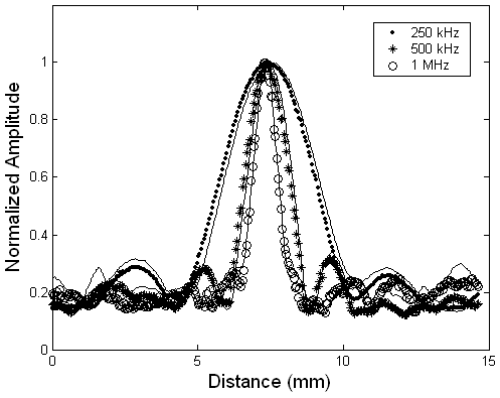

Fig. 4. Time reversal spatial focusing pattern along axis X for different frequencies. ●: 250 kHz, ✻: 500 kHz, ○: 1 MHz (lines: simulations; symbols: experiments).

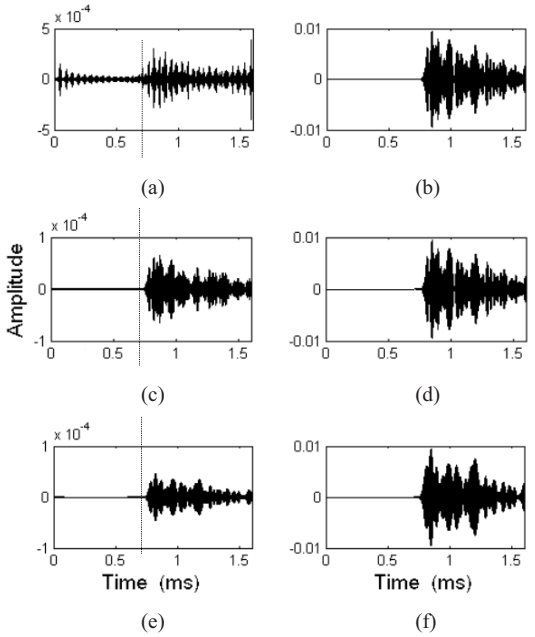

Fig. 5. Estimated transfer functions (a, c, e) and estimated direct signals (b, d, f) for various regularization parameters for 500 kHz (q=-1 for a and b, $q=10^3$ for c and d and $q=10^7$ for e and f).

The transfer function (or impulse system response) has to start after the initial pulse at time $t>t_0$ (see Fig. 5), but the estimation of the transfer function for low value of q gives the presence of impulse response before t_0 which is physically incorrect. High values of q give sufficient difference between estimated and measured signals, so it could be some optimal value of the regularization parameter.

To select an optimum value of the regularization parameter, we used two criteria:

1. The criterion of proximity of measured and estimated signals. A correlation coefficient $K=s_{est}(t)*s(t)$ between the measured signal $s(t)$ and estimated signal $s_{est}(t)$ has to be close to unity. Figure 6a shows the calculated dependence of K on the parameter of regularization q.
2. The small value of the transfer function before the initial pulse ($t<t_0$). For minimization of the signal at time $t<t_0$ we use parameter N, which is the ratio of estimated energy impulse response for $t<t_0$ to energy for $t<t_0$:

$$N = \frac{\int_0^{t_0} h_{est}^2 dt}{\int_{t_0}^{t_{delay}} h_{est}^2 dt}$$

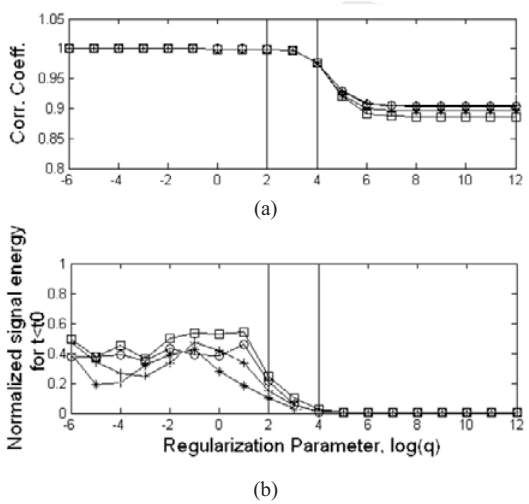

Fig. 6. Dependence of cross correlation between estimated and measured direct signals K and normalized level of estimated transfer function N for $t<t_0$ on parameter q. Different lines present different transducers.

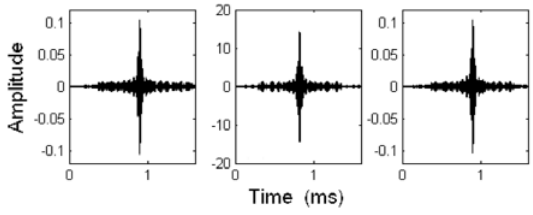

Fig. 7. Comparison of the experimentally measured TRA-focused wave for signal with carrier frequency of 500kHz and half period sinusoidal envelope with predicted one: a) experiment, b) estimation using autocorrelation of the received signal(Eq.(12)), c) estimation using full formulae (13).

Fig. 6(b) shows the dependence of this parameter N on the parameter of regularization q.

As seen from Fig. 6. the choice of parameter q around 1000 provides a good correlation between estimated and measured direct signals and low level of estimated impulse response for $t<t_0$.

This value of q was used for prediction of TRA-focused signal, according to Eq. (13). The results of calculation are presented in Fig. 7(c). Fig. 7(a) shows the form of TRA-focused signal observed in the experiment and Fig. 7(b) the form of calculated signal according to approximate formula (12). It is seen that the TRA-focused wave form calculated according to Eq. (13) is practically identical to the waveform observed in the experiment.

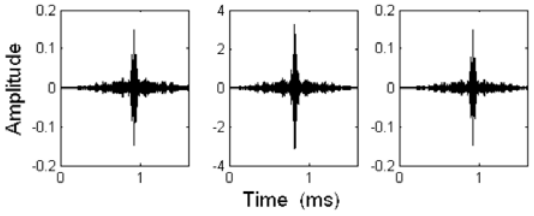

(a) (b) (c)

Fig. 8. Comparison of the experimentally measured TRA-focused wave for single period of frequency 500 kHz signal with predicted one: a) experiment, b) estimation using autocorrelation of the received signal(Eq.(12)) , c) estimation using full formulae (13).

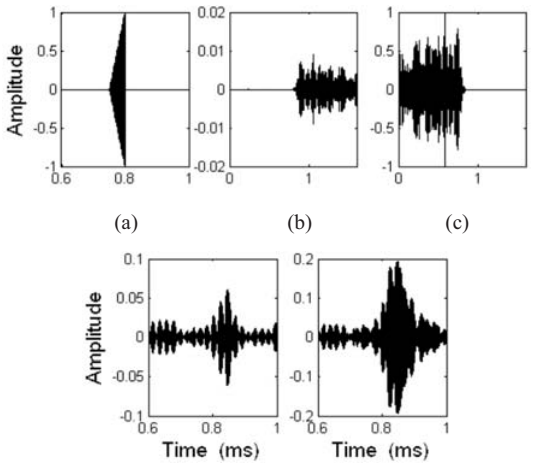

(a) (b) (c)

(d) (e)

Fig. 9. The snap shots of the signal in the process of TRA focusing of tone burst signal with carrier frequency of 500 kHz and triangular envelope: a) step 1 - initial radiated signal e(t), b) step 2 – recorded long reverberating signal s(t), c) step 3 – time reversal normalized signal prepared for reradiation, d) TRA-focused signal radiated by a single transducer, e) TRA-focused signal radiated by all five transducers.

Fig. 8 presents another example for a short pulse focusing when initial signal *e(t)* is one period of sinusoid with frequency of 500 kHz. The results of estimation are also close to the experiment. There is a small difference between the experimental waveform and that calculated with the use of approximate equation (12) and practically full coincidence for that calculated from Eq. (13).

The prediction of the spatial structure if the TRA-focused signal was performed according to Eq. (14) and the results of calculations presented in Fig. 4 are close to the experimental results.

5. Formation of arbitrary waveforms in TRA focusing system

Here, we consider the opportunity of arbitrary waveform formation with the TRA-focused system. As an example let us consider an experiment for TRA focusing of the signal with carrier frequency of 500 kHz and triangular envelope as shown in Fig. 9. All steps of the TRA focusing of this signal are presented in Fig. 9 and it is seen that the TRA-focused signal waveform is far from the initial signal waveform.

The measurements of the transfer function allow producing a TRA-focused signal with the desired waveform. Let us find what signal *x(t)* we have to apply to the transducer to get the desired signal *y(t)* in the TRA focus. These two signals are connected through an impulse response function

$$y(t) = x_j(t) \otimes h_j(t) . \tag{17}$$

In spectral form this expression is:

$$Y(\omega) = X_j(\omega)\ H_j(\omega) . \tag{18}$$

Using Eq. (7) for transfer function spectrum $H_j(\omega)$, one can find the spectrum of a function that can be applied for generation of the desired waveform:

$$X_j(\omega)\ = \frac{E\ (\omega)Y(\omega)}{S_j(\omega)} . \tag{19}$$

The calculation of the applied signal that produces the desired waveform in the focus can be done by using the same regularization method:

$$x_j(t) = F^{-1}\left(\frac{E\ (\omega)Y(\omega)S_j^*\ (\omega)}{S_j(\omega)\ S_j^* + q} \right), \tag{20}$$

where q is the regularization parameter.

The estimated TRA-focused signal can be calculated according to the expression:

$$p_j(t) = F^{-1}\left(\frac{Y(\omega)S_j^*\ (\omega)S_j\ (\omega)}{S_j(\omega)\ S_j^* + q} \right). \tag{21}$$

As an example, let us consider a triangular waveform as a desired signal at a focal point. Fig. 10 presents the estimated radiated signals *x(t)* TRA-focused signals calculated for various values of the regularization parameter.

For small values of the regularization parameter, the form of the TRA-focused signal is close to the desired triangular waveform but the amplitude of the

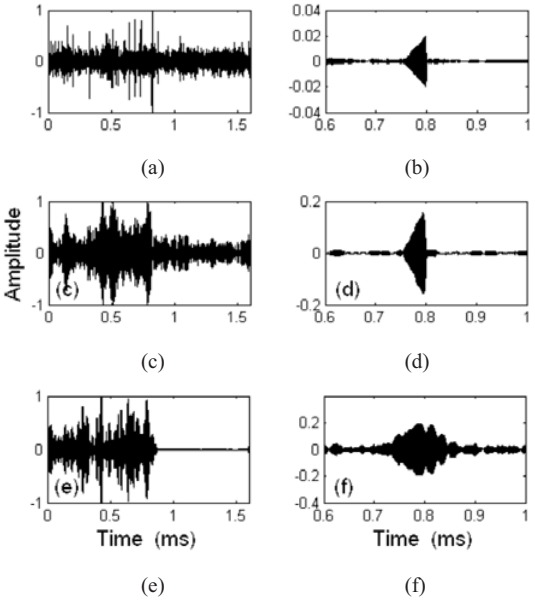

Fig. 10. Estimated applied signals x(t) (a, c, e) and experimentally observed signal at focal point (b, d, f) for various regularization parameters, (q=-6 for a and b, q=-2 for c and d and q=2 for e and f).

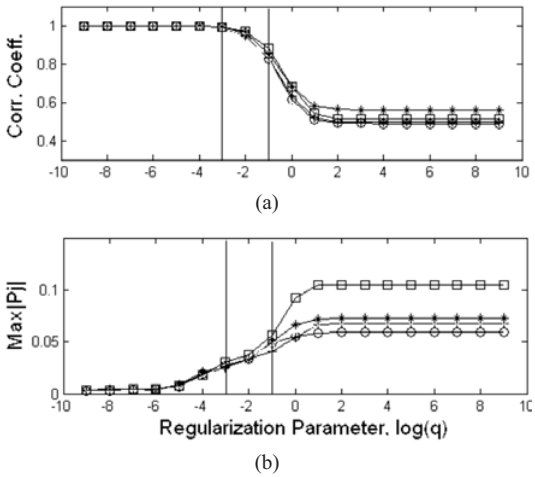

Fig. 11. Dependence of the correlation coefficient (a) and TRA-focused signal amplitude (b) on the regularization parameter. Different lines present different transducers.

signal is small. For higher q the amplitude increases but the waveform becomes far from the desired waveform.

To select an optimum value of the regularization parameter, we used two criteria similar to the criteria used in the previous case:

1. The criterion of proximity of measured and estimated signals. The correlation coefficient K between the estimated TRA-focused signal $p(t)$ and desired signal $y(t)$ has to be close to unity. This coefficient was calculated according to the formula:

$$K = p_j(t) * y(t) = F^{-1}\left(\frac{Y(\omega)Y^*(\omega)S_j^*(\omega)S_j(\omega)}{S_j(\omega)\,S_j^* + q}\right) \quad (22)$$

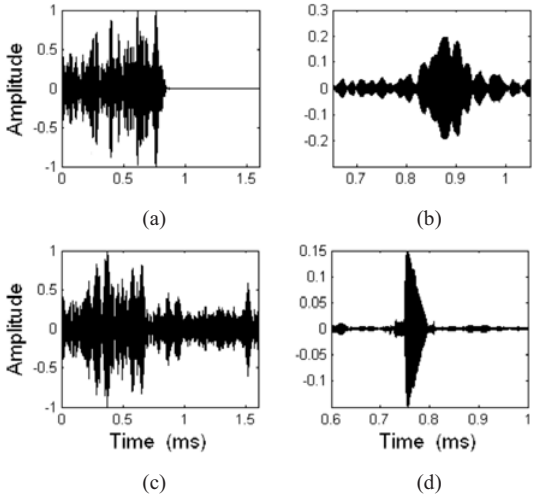

Fig. 12. Comparison between normal TRA method and improved waveform focusing for tone-burst signal with positive ramp triangular envelope: a) normal TRA reradiated signal, b) TRA-focused signal for normal TRA procedure c) improved signal x(t) applied to transducer, d) improved focused signal.

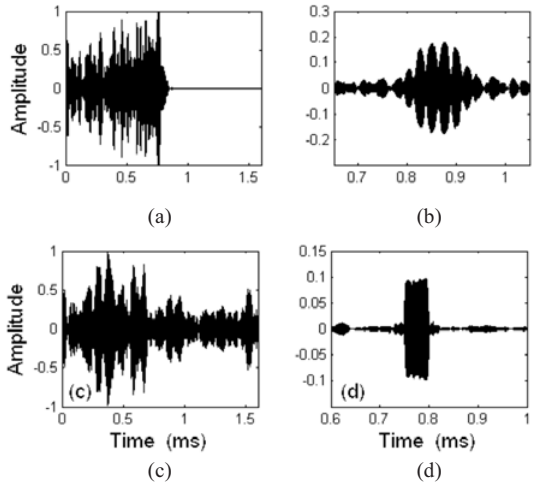

Fig. 13. Comparison between normal TRA method and improved waveform focusing for tone-burst signal with rectangular envelope: a) normal TRA reradiated signal, b) TRA-focused signal for normal TRA procedure c) improved signal x(t) applied to transducer, d) improved focused signal.

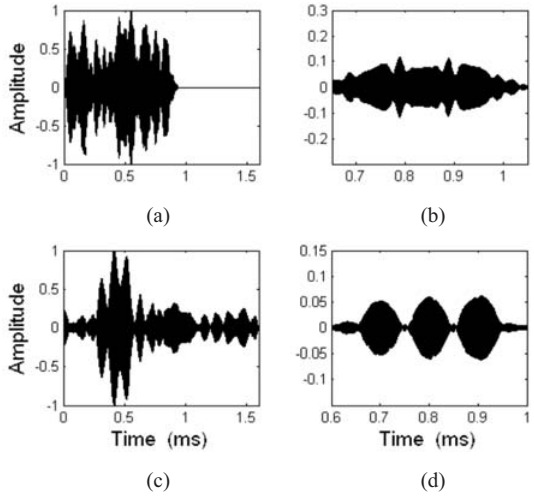

Fig. 14. Comparison between normal TRA method and improved waveform focusing for tone-burst signal with envelope modulated by 5 kHz: a) normal TRA reradiated signal, b) TRA-focused signal for normal TRA procedure c) improved signal x(t) applied to transducer, d) improved focused signal.

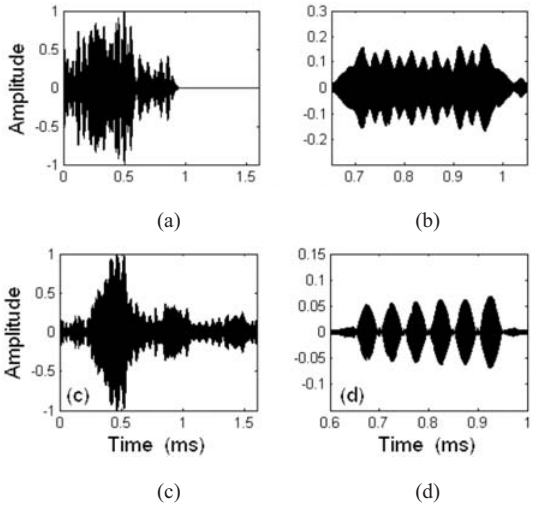

Fig. 15. Comparison between normal TRA method and improved waveform focusing for tone-burst signal with envelope modulated by 10 kHz: a) normal TRA reradiated signal, b) TRA-focused signal for normal TRA procedure c) improved signal x(t) applied to transducer, d) improved focused signal.

2. The second criterion is the amplitude of calculated TRA-focused signal.

Fig. 11 shows the calculated dependence of the correlation coefficient K and TRA-focused signal amplitude on parameter of regularization q. It is seen that a waveform close to the desired triangular signal and large amplitude in the focus can be reached for q=0.01.

The application of the developed method for producing various waveforms in the focus of the TRA-focused system is illustrated in Figs. 12-15. Figs. 14 and 15 present the formation of amplitude-modulated signals.

6. Conclusion

A method was developed to predict the TRA-focused waveform and formation of the desired waveform based on the measurements of transfer function between the transmitter and the focus point. The estimated waveforms and spatial TRA-focused field distribution were practically identical to that observed in the conducted TRA experiment. The method was used for focusing of triangular, rectangular, and amplitude modulated tone burst signals with different frequencies. The level of side lobes in the generated signals was much lower than that for standard TRA focusing. Time reversal sensing technique was investigated as tool for structural health monitoring [18]. We hope that this research will be constructive for ultrasound focusing in various areas.

References

[1] M. Fink, Time reversed acoustics, *Scientific American,* November (1999) 91-97.

[2] M. Fink, D. Cassereau, A. Derode, C. Prada, P. Roux, M. Tanter, J. Thomas and F. Wu, Time-reversed acoustics, *Reports on Progress in Physics* 63 (2000) 1933-1995.

[3] M. Fink, G. Montaldo and M. Tanter, Time-reversal acoustics in biomedical engineering, *Annu. Rev. Biomed. Eng.* 5 (2003) 465-497.

[4] G. Montaldo, D. Palacio, M. Tanter and M. Fink, Building three-dimensional images using a time-reversal chaotic cavity, *IEEE Transactions on Ultrasonics, Ferroelectrics, and Frequency Control.* 52 (9) (2005) 1489-1497.

[5] G. Montaldo, D. Palacio, M. Tanter and M. Fink, Time reversal kaleidoscope: A smart transducer for three-dimensional ultrasonic imaging, *Applied Physics Letters* 84 (19) (2004) 3879-3881.

[6] A. J. Devaney, E. A. Marengo and F. K. Gruber, Time-reversal-based imaging and inverse scattering of multiply scattering point targets, *J. Acoust. Soc.*

Am. 118 (5) (2005) 3129-3138.

[7] C. Prada, E. Kerbrat, D. Cassereau and M. Fink, Time reversal techniques in ultrasonic nondestructive testing of scattering media, *Inverse Problems* 18 (2002) 1761–1773.

[8] N. Chakroun, M. Fink and F. Wu, Time reversal processing in nondestructive testing, *IEEE Trans. Ultrason. Ferroelec. Freq. Contr.* 42 (1995) 1087-1098.

[9] T. J. Ulrich, P. A. Johnson and A. Sutin, Imaging nonlinear scatterers applying the time reversal mirror, *J. Acoust. Soc. Am.* 119 (3) (2006) 1514-1518.

[10] A. M. Sutin and P. A. Johnson, Nonlinear elastic wave NDE II: Nonlinear wave modulation spectroscopy and nonlinear time reversed acoustics, *Review of Quantitative Nondestructive Evaluation* edited by D. O. Thompson and D. E. Chimenti, AIP, New York 24 (2005) 385-392.

[11] A. Sutin, P. Johnson, J. TenCate and A. Sarvazyan, Time reversal acousto-seismic method for land mine detection, Proc. SPIE: Detection and Remediation Technologies for Mines and Minelike Targets X 5794 (2005) 706-716.

[12] P. D. Norville and W. R. Scott Jr., Time-reversal focusing of elastic surface waves, *J Acoust. Soc. Am.* 118 (2) (2005) 735-744.

[13] B. Libbey and D. Fenneman, Acoustic to seismic ground excitation using time reversal, Proc. SPIE: Detection and Remediation Technologies for Mines and Minelike Targets X, R. S. Harmon, Ed., 5794 (2005) 643-654.

[14] A. Sutin and A. Sarvazyan, Spatial and temporal concentrating of ultrasound energy in complex systems by single transmitter using time reversal principles, Proceeding of the World Congress on Ultrasonics, Paris, September (2003) 863-866.

[15] V. Bertaix, J. Garson, N. Quieffin, S. Catheline, J. Derosny and M. Fink, Time-reversal breaking of acoustic waves in a cavity, *Am. J. Phys.* 72 (10) (2004) 1308-1311.

[16] J. Ching, A. C. To and S. D. Glaser, Microseismic source deconvolution: Wiener filter versus minimax, Fourier versus wavelets, and linear versus nonlinear, *J. Acoust. Soc. Am.* 115 (6) (2004) 3048-3058.

[17] G. Montaldo, M. Tanter and M. Fink, Real time inverse filter focusing through iterative time reversal, *J. Acoust. Soc. Am.* 115 (2) (2004) 768-775.

[18] H. W. Park, S. B. Kim and H. Sohn, Time Reversal Sensing for Structural Health Monitoring, Korea Institute for Structural Maintenance Inspection (KSMI), (2005) 427-432.